FEATURES OF LASER-MACHINED MICRO-TEXTURES ON THE SURFACE OF CEMENTED CARBIDE TOOL

QUAN WAN * **, MINLI ZHENG, SHUCAI YANG, WEIWEI LIU**
¹School of Mechatronics Engineering, Harbin University of Science and Technology, Harbin, China.

Micro-texturing can greatly improve the cutting performance of tools. Thus, this paper attempts to disclose the effects of laser machining on the morphology and surface performance of micro-textured tools. Firstly, the 2D and 3D morphologies of micro-textures were explored and the effects of different laser machining parameters were analyzed. After that, the author examined the microstructure and the composition of the heat affected zone (HAZ) around each micro-texture. Furthermore, the micro-hardness and nano-hardness in different areas of HAZ were subjected to comparative analysis. The results show that laser parameters directly affect the micro-texture morphology and surface material properties. With the same total energy, high power density and the number of scans can reduce the deposition of sputtering materials, improve the size accuracy of micro-texture, and increase the performance of micro-texture surface materials. The research findings lay the basis for the fabrication of micro-textured cemented carbide cutting tools.

Keywords: Cemented Carbide Tool; Micro-Textured Surface; Laser Machining; Heat Affected Zone (HAZ)

1. Introduction

The micro-textures on the rake and flank faces of the cutting tool can minimize the effective contact area and reserve lubricant, thus reducing the chip-tool friction and enhancing the cutting performance. The friction reduction is accompanied by the attenuation of cutting forces and temperature, as well as the growth in wear resistance and tool life [1, 2].

Much research has been done on surface micro-textured tools. For instance, Sugihara et al. [3, 4] investigated the positive impacts of textured surfaces on the anti-adhesion effect and lubricity of the cutting tool surface during the machining of lightweight aluminum-based composites, and fabricated a cubic boron nitride (CBN) cutting tool with textured flank face for high-speed machining of Inconel 718, which can stabilize the adhesion layer and extend the tool life. Kümmel [5] attempted to improve the wear resistance and stabilize the built-up edge of textured cemented carbide cutting tools.

With good wear resistance, surface textured tools provide a solution to cutting difficult-to-machine materials. Yang [6] explored the cutting performance of cemented carbide tools with microgrooves on Ti-6Al-4V titanium alloy. Xing [7] analyzed many cutting parameters of textured Al_2O_3/TiC ceramic tools in dry cutting of hardened steel, including tool wear, cutting force, cutting temperature, friction coefficient, surface roughness and chip morphology. Liu [8] improved flank wear resistance with microscale grooves textured tools for dry cutting of green alumina ceramics.

Many scholars have probed into the effects of micro-texture type, shape, layout and dimension on the improvement of cutting performance. For

example, Obikawa et al. [9] compared the machinability of aluminum alloy between perpendicular, parallel, pit, and square dot surface micro-textures, revealing that parallel and square dot are the most effective micro-texture types to improve the lubrication conditions. Kim [10] confirmed the significant effect of micro-texture type on the chip flow angle, and identified the most effective shape and size for the minimum cutting force. Kawasegi [11] found that lower cutting forces can be achieved when the texture is perpendicular rather than parallel to the chip flow direction. Through finite-element simulation, Ma et al. [12, 13] examined the performance of microgroove and micro-bump textured cutting tools, noting that the width, depth, and the distance from cutting edge of the two micro-textures all have influence on cutting forces.

In addition, many methods have been proposed to fabricate micro-textures. P. Koshy [14] produced micro-textures by electrical discharge machining (EDM). Kawasegi [15] created a texture on the rake face of a diamond tool, using radiation of focused ion beam and heat treatment. Fatima [16] generated micro- and nano-textures with the aid of a femtosecond laser. Zhu [17] proposed an innovative fabrication plan for superior microgrooves: texturing with ultrasonic elliptical vibration. Xie [18] adopted a micro-grinding approach to realize the accurate control over the shape of micron-scale grooves. Li [19] combined micro-EDM and high-frequency vibration to fabricate micro holes and linear grooves, and proved that the combined method can achieve high dimensional accuracy and accurate positioning.

In recent years, friction stir processing (FSP) has been successfully applied to AISI 52100

* Autor corespondent/*Corresponding author*,
E-mail: wq@hrbust.edu.cn

steel. The results show that FSP can improve microhardness and wear resistance [20]. In the laser melting zone, the hardness of the Mg-11Y-2.5Zn alloy is slightly improved, and the laser melting surface has significant wear resistance [21]. After electron beam processing, the results of 40Cr material showed a significant increase in surface roughness and hardness [22]. The effects of external thermodynamic effects on the properties of the microstructure are mentioned in these studies, and the laser-induced cemented carbide is in accordance with the principle of thermodynamic effects.

Laser ablation of cemented carbide tools has become a new method, which is a process of thermal processing. The results of some research show that the tool life after laser heat treatment is 20% higher than that of the tool without heat treatment [23, 24]. Wen et al. [25] tested the microtexture properties of the TC4 heat affected zone (HAZ) on the substrate. The results show that multiple remelting can effectively eliminate the quenching structure of HAZ, and remelting multiple thermal cycles has a great influence on the performance of HAZ, especially hardness. Studies by Popoola et al. [26] show that the surface micro-texture after laser processing of X12CrNiMo Steel becomes dense, and the surface friction coefficient is reduced compared with untreated.

As above, the micro-texture tools and their cutting performance have long been research hotspots. Many scholars have employed these tools to improve the cutting performance and tool life, and realized the desired micro-texture shape and dimensions by adjusting machining parameters. The existing studies mainly concentrate on the following three aspects: the antifriction performance of micro-texture tools, the layout and dimensions of micro-textures, and the fabrication methods of micro-textures.

Nevertheless, these studies only tackle the 2D conditions of micro-textures, failing to address the 3D morphology (i.e. 2D morphology + depth). Meanwhile, the positive effects of micro-textures on cutting performance have only been analyzed in terms of tool friction and wear. There is no report on how the fabricating process of micro-textures change the textured surface performance of cutting tools. Actually, the intense thermomechanical effects of micro-texture fabrication have a significant impact on the surface properties of cutting tool, which in turn bears on the chip-tool interaction and the cutting performance.

In light of the above, this paper attempts to confirm the morphology of 3D micro-textures and disclose the variation in tool surface properties after laser cutting of micro-textures on the rake face of cutting tool. Firstly, micro-textures were machined at different laser parameters, the 2D and 3D morphologies of the textures were identified, and the effects of laser parameters on the

morphologies were discussed in details. After that, the author investigated the laser machined microstructure and composition of the heat affected zone (HAZ), which emerged under the thermal effect of laser machining. Furthermore, the micro-hardness and nano-hardness in different areas of HAZ were subjected to comparative analysis.

The research findings shed new light on how surface performance helps improve the cutting performance of surface textured tools.

2. Laser Machining of Micro-Texture on Cemented Carbide Cutting Tool

This section is about the laser machining of micro-textures on the rake face of a YG8 cemented carbide cutting tool, which consists of a tungsten carbide (WC) matrix and 8% Co adhesive. The parameters of laser machining are listed in Table 1 below.

Table 1

Laser machining parameters

Type	ZT-Q-50
Laser type	Fiber laser
Frequency	20-80 (kHz)
Power range	10–100%
Average output power	50 (W)
Marking depth	0.3-1 (mm)

A series of circular pit micro-textures with a certain depth were machined on the rake surface of the YG8 cemented carbide tool near the main cutting edge. The fiber laser parameters, including spot diameter D, power P, scanning speed V and the number of scanning cycles N, were adjusted during the machining process. Here, a four-factor, four-level orthogonal test is designed with the parameter settings shown in Table 2. The mean laser power density P_{av}, the mean laser output energy E_{av}, and the total laser output energy E_{total} can be calculated as:

$$P_{av} = P / \pi r^2$$
$$E_{av} = Pt = 2Pr / v \qquad (1)$$
$$E_{total} = NE_{av}$$

where t is the time of one scanning cycle; r is the spot radius. The results of equation (1) are given in Table 2.

After laser machining, the micro-textured tool surface was cleaned by ultrasonic wave for 8min, and then cooled down to the ambient temperature 20°C. Next, the morphology of the micro-textures was observed by a VHX-1000 ultra-depth microscope (UDM) and a HITACHI SU3500 scanning electron microscope

Quan Wan, Minli Zheng, Shucai Yang, Weiwei Liu / Features of laser-machined micro-textures on the surface of cemented carbide tool

253

Orthogonal test parameters

ID	D (μm)	N	P (W)	v (m/min)	$P_{av}(10^6 W/cm^2)$	t $(10^{-5}s)$	E_{av} (mJ)	E_{tatal}(mJ)
1	40	3	30	25	2.39	9.6	2.88	8.64
2	40	5	37	50	2.95	4.8	1.78	8.88
3	40	8	45	75	3.58	3.2	1.44	11.52
4	40	10	50	100	3.98	2.4	1.20	12
5	50	3	37	75	1.89	4.0	1.48	4.44
6	50	5	30	100	1.53	3.0	0.90	4.5
7	50	8	50	25	2.55	12.0	6.00	48
8	50	10	45	50	2.29	6.0	2.70	27
9	60	3	45	100	1.59	3.6	1.62	4.86
10	60	5	50	75	1.77	4.8	2.40	12
11	60	8	30	50	1.06	7.2	2.16	17.28
12	60	10	37	25	1.31	14.4	5.33	53.28
13	70	3	50	50	1.30	8.4	4.20	12.6
14	70	5	45	25	1.17	16.8	7.56	37.8
15	70	8	37	100	0.96	4.2	1.55	12.43
16	70	10	30	75	0.78	5.6	1.68	16.8

(SEM), while the hardness of the micro-textured surface was measured by HXD-1000 nano- and micro-hardness testers.

3. Results and Discussion

3.1. Morphology analysis

Figure 1 presents the 2D and 3D morphologies of the laser-machined micro-textures by the UDM and the SEM. It can be seen that the material inside the micro-textures melted, while the surface region around each micro-texture was subjected to different degrees of ablation. These changes are attributable to the heat action of the laser beam.
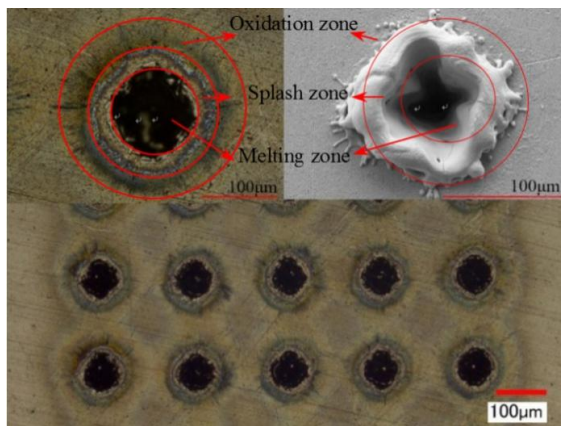

Fig. 1 - UDM and SEM images on the morphology of micro-textures.

According to Table 1, the mean power density P_{av} was on the order of 10^6 W/cm². Under the high power density, the tool surface material was fused and gasified. Then, forming a micro-hole known as the melting zone by the gas pressure. Meanwhile, lots of molten materials accumulated around the micro-textures, creating a splashed zone, with a small amount attached to the surface outside the splashed zone. In addition, the high temperature of laser machining oxidized the

elements on the tool surface, and thus left an oxidation zone. The splashed zone and oxidation zone together formed the HAZ around each micro-texture.

The 3D morphology of micro-textures was obtained by the UDM and shown in Figure 2. The 3D contour reveals that the laser machined micro-textures had a conical shape: wider in the top than the bottom. This is because laser energy is negatively correlated with the texture depth. In Figure 2, AB is the micro-texture depth and CD is the micro-texture diameter on tool surface. The size and height of the splashed zone can be obtained according to the morphology of that zone in the convex part outside the CD. The oxidation zone lies further away, outside the splashed zone. Thus, the dimensions of each micro-texture and its surrounding HAZ can be determined according to the UDM results.

Figure 3 displays the 3D morphology of micro-textures observed by the UDM under different laser machining parameters. The total input energy of the laser beam gradually decreased from Figure 3(a) to Figure 3(d), but remained the same from Figure 3(e) to Figure 3(h).

It can be seen from Figures 3(a)~3(d) that the growing laser energy led to an increase in the micro-texture size. This trend obeys the law of the conservation of energy, i.e. more materials are removed after more energy is absorbed. However, the total input energy has nothing to do with the intensity range of laser interaction on cemented carbide material.

Furthermore, with increase of laser power density, more and more materials accumulated around each micro-texture, whose conical degree was in a decline. The possible reasons for these phenomena are as follows: the materials were more intensely gasified and melted with the growth of laser power density; the molten materials were splashed out rapidly and accumulated around the micro-textures. Meanwhile, the micro-texture was less conical as the laser penetrated deeper into
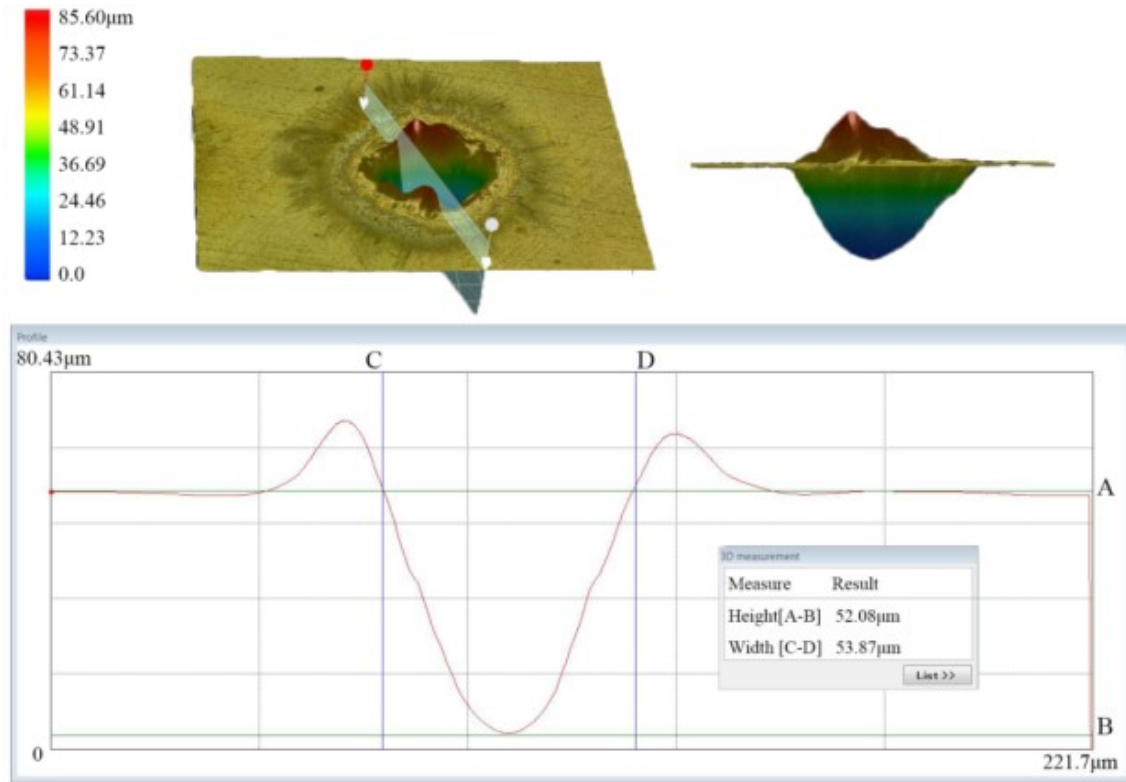
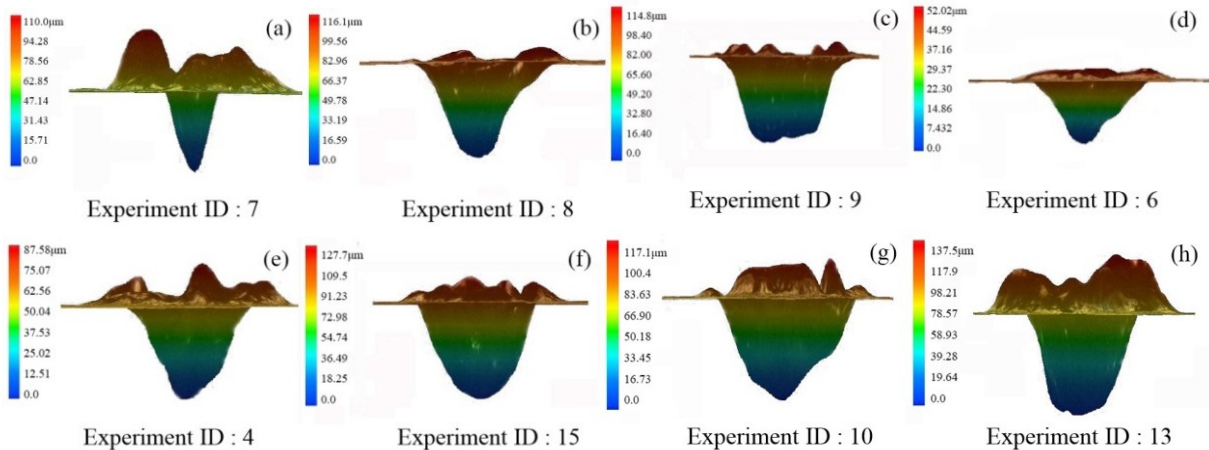Fig. 2 - UDM images on the 3D morphology of micro-textures.

Fig. 3 - 3D morphology of micro-textures at different machining parameters.

the material, thanks to the high power density. Thus, it can be concluded that the intensity range of laser interaction with tool material depends directly on laser power density.

Despite the constancy of total input energy, the amount of materials accumulated in the splashed zone was on the rise from Figure 3(e) to Figure 3(h). Coupled with the data in Table 1, it can be seen that the amount of accumulated materials is related to the input energy per cycle. The higher input energy per cycle, the more intense the laser interaction with the material, and the greater the amount of accumulated materials in the splashed zone. Further analysis shows that the micro-textures were less conical with the growth in the

time per cycle, because the tool material was ablated and melted more thoroughly through a longer scanning cycle.

Figure 4 presents a series of SEM images on the micro-textures machined by 70µm laser spot. The spot diameter remained the same, while the laser power reduce, and thus the laser power density, was reduced continuously. As shown in Figure 4, the splashed zone and oxidation zone around each micro-texture shrank gradually with the laser power density. The correlation agrees well with the UDM results in Figure 3. Hence, it is safe to say that laser power density directly bears on the HAZ around each micro-texture of cemented carbide tool.
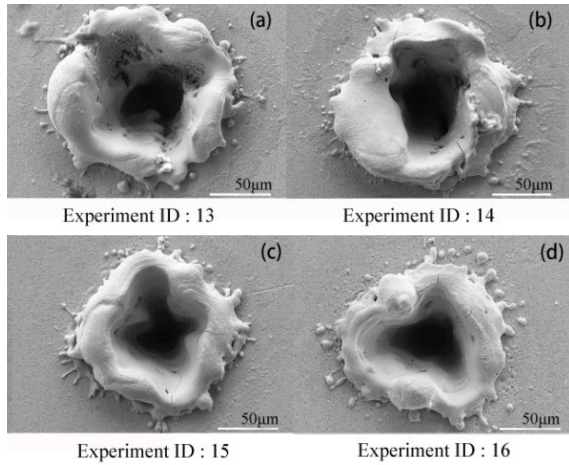
Fig. 4 - SEM images on the 3D morphology of micro-textures.

3.2 HAZ microstructure analysis

The YG8 cemented carbide cutting tool mainly contains hard-phase WC and bonding-phase Co. The HAZ microstructure on the laser-machined tool surface is displayed in Figure 5, where the bright area is the WC and the dark area is the Co. Obviously, the hard-phase WC became increasingly triangular and polygonal. After the laser machining, an oxide film layer was attached on the surface around each micro-texture, as shown in the red circle in Figure 5(a). The oxide film layer has a loose pore structure. By contrast, there was no obvious loose oxide film layer in Figure 5(b). The difference comes from the fact that the HAZ properties and the intensity range of laser interaction with tool material both vary with the laser parameters (e.g. laser power density and input energy) during laser machining (Section 3.1). Moreover, the surface of the cemented carbide cutting tool may react with the oxygen in the air, under the high temperature produced in laser machining.

As shown in Figure 5(b), a small amount of molten materials was attached to the micro-textured surface due to the low laser power density. However, there was still a certain degree of oxidation in this region under laser heating. The surface morphology in Figure 5 also shows that the HAZ was more porous than the matrix not affected by the laser, for the bonding phase Co, whose boiling point is much lower than the hard-phase WC, was partially gasified under the heat of laser machining.

3.3 HAZ surface composition analysis

The element composition of the HAZ (Figure 6) around each micro-texture was analyzed by the surface energy dispersion spectrum (EDS). The cemented carbide is mainly composed of such elements as W, Co, C, O and Ti. As shown in Figure 6, the circular HAZ had much higher contents of Co and O than the unaffected region, and similar contents of the other elements with the latter.
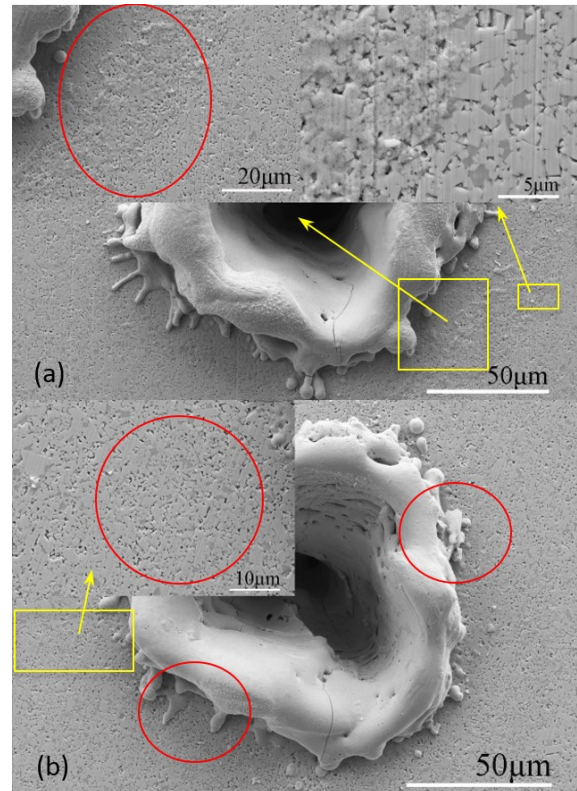

Fig. 5 - SEM images on the HAZ microstructure.

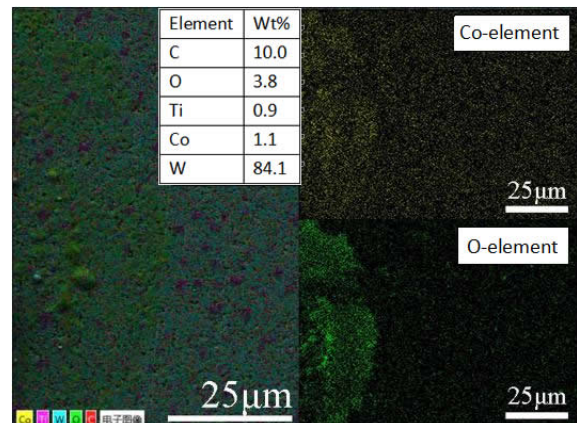| Element	Wt%
C	10.0
O	3.8
Ti	0.9
Co	1.1
W	84.1

Fig. 6 - Surface EDS of the HAZ.

The composition difference and similarity demonstrated the severe oxidation of the cemented carbide during laser machining. Specifically, the hard-phase WC is relatively stable under high temperature and unlikely to react with the oxygen in the air. However, the bonding-phase Co is prone to oxidation. The oxidation products are CoO and Co_3O_4 at above 300°C, and only CoO at above 900°C. Hence, the materials attached to the oxidation zone on the tool surface shuould be the oxides of Co.

The HAZ composition was also analyzed by the line energy spectrum Figure 7. Since the oxides of Co are the main component of the HAZ, this part focuses on the variation in the amount of

(a)   Experiment ID : 7
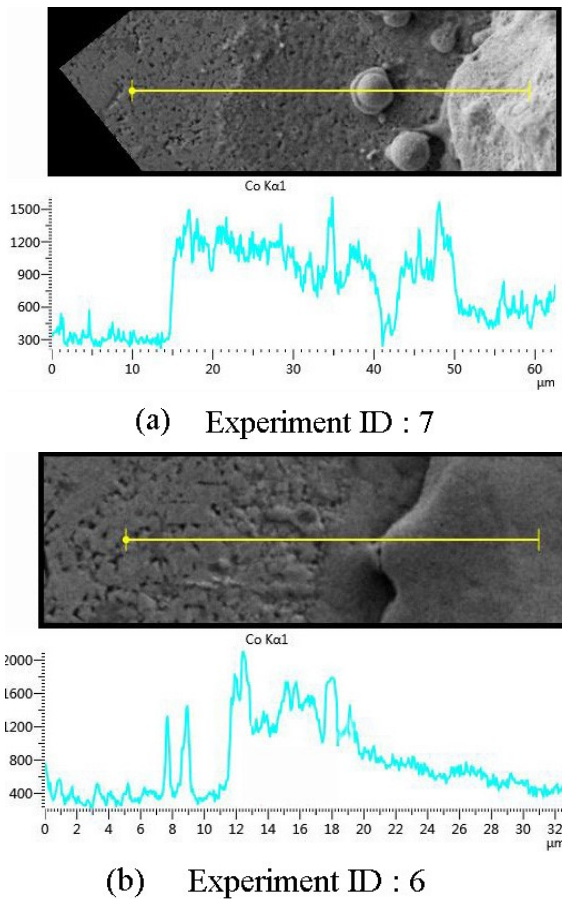

(b)   Experiment ID : 6

Fig. 7 - Variation in the amount of Co element in the HAZ.

Co element in this zone. It can be observed that the Co content exhibited an inverted U shape trend with the increase in the distance to the micro-texture center. The amount of Co element in the oxidation zone was much higher than that in the splashed zone and the unaffected zone. Below is the possible reason for these phenomena. Due to the Gaussian distribution of the laser power, the splashed zone near the micro-texture center was heated to a very high temperature. In this zone, the Co content declined as the element, with a low boiling point, was partially gasified under the intense laser. In the oxidation zone, the Co element was highly oxidized as the temperature decreased from the central area to the oxidation zone. The content of Co oxides was reduced as the temperature further dropped from the oxidation zone to the peripheral areas.

Comparing Figures 7(a) and 7(b), it is learned that more Co elements were present in the oxidation zone of the latter figure. The laser parameters in Table 1 show that the laser power is more intense in Figure 7(b) than in Figure 7(a). This means the laser interaction with the material increases with the laser power density, leading to the high temperature and intense Co gasification in Figure 7(a).

3.4. Analysis of nano- and micro-hardness of the HAZ

The surface hardness of the HAZ were measured by nano- and micro-hardness indenters to disclose the effects of temperature on HAZ mechanical properties. The materials accumulated in the splashed zone were removed to ensure the surface flatness and minimize the surface friction.

Figure 8 shows the nano-hardness of the matrix in the cutting tool, which is not laser-machined. It can be seen that the nano-hardness of the matrix material increased with the indentation depth, and stabilized at 20.264GPa when the depth reached 200nm.
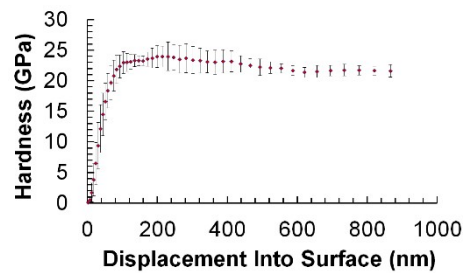

Fig. 8 - Nano-hardness of the matrix of original cutting tool.
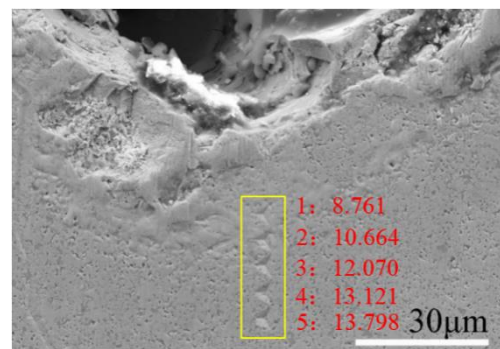

Fig. 9 - Nano-hardness in the HAZ of laser-machined cutting tool.

Figure 9 depicts the nano-hardness at different positions of the HAZ in a laser-machined tool. Compared with Figure 8, it can be observed that the nano-hardness in the HAZ after laser machining was obviously lower than that of the matrix, and gradually increased from the center to the edge of the HAZ. The observed results can be explained by the loose oxide film, which becomes thinner and thinner from the inside to the outside, over the oxidation zone after laser machining (Sections 3.2 and 3.3).

Nevertheless, nano-hardness measurement cannot accurately grasp the penetration depth of the laser, which hinders the analysis on the tool surface performance after laser machining. To solve the problem, the laser-machined tool was measured by a micro-hardness indenter, aiming to
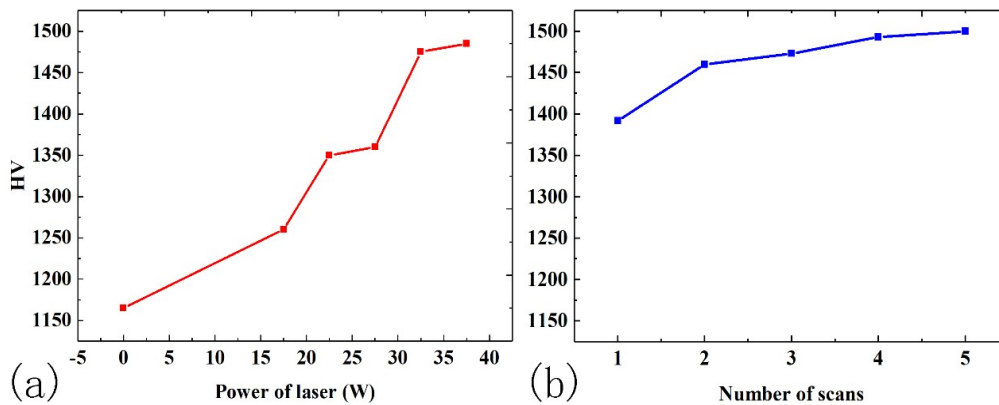
Quan Wan, Minli Zheng, Shucai Yang, Weiwei Liu / Features of laser-machined micro-textures on the surface of cemented carbide tool

257

Fig. 10 - Micro-hardess of the cemented carbide tool surface (a)The relationship between micro-hardness and laser power (b)The relationship between micro-hardness and the number of scanning cycles.

disclose the effect of temperature on the HAZ. Figure 10 records the measured micro-hardness of the cemented carbide tool surface after being machined with different laser parameters.

Figures 10(a) and 10 (b) respectively show the relationship between micro- hardness and laser power (pre-machining value: 0W) and that between micro-hardness and the number of scanning cycles. It can be seen from Figure 10 that the HAZ micro-hardness increased with the laser power in the machining process, and grew with the number of scanning cycles. The relationships are attributable to the following reasons. More laser power and scanning cycles mean more laser heat being transferred to the tool material. During laser machining, the rapid heating and cooling creates a quenching-like effect: the surface microstructure was changed and the grains were refined, pushing up the micro-hardness in the HAZ. Meanwhile, under the heat of laser machining, the bonding phase Co, whose boiling point is much lower than the hard-phase WC, was partially gasified under the heat of laser machining (Section 3.2).

4. Conclusions

Considering the positive effects of laser-machined micro-textures on the cutting performance, this paper probes into the 2D and 3D morphologies of micro-textures on cutting tool after laser machining, and analyzes the such features of the HAZ around each micro-texture as element content, nano-hardness and micro-hardness. The following conclusions were obtained through this research:
The laser power density directly affects the heat affected zone of the micro-texture of cemented carbide tools. The characteristics and range of the heat affected zone vary with changes in laser parameters such as laser power density and input energy. The increase in laser energy results in an increase in the size of the microtexture. At the same time, the amount of sputtered material deposited is related to the input energy of each

cycle. As the input energy per cycle increases, more material builds up in the splash zone.

The hard alloy is severely oxidized during laser processing, and the surface of the HAZ is covered with loose oxides of Co. With the increase of the distance from the center of the micro-texture, the cobalt content is in an inverted U-shape, and the cobalt content in the oxidation zone is significantly higher than that in the splashed zone and the unaffected zone.
The laser heat helps improve the microstructure of the HAZ and thus the surface performance of the cutting tool, due to the refinement of the HAZ microstructure and growing micro-hardness of tool material under high temperature.

REFERENCES

1. T. Sugihara, T. Enomoto, Crater and flank wear resistance of cutting tools having micro textured surfaces. Precision Engineering, 2013, **37**(4), 888–896.
2. M.T. Pamuk, A. Savaş, Ö. Seçgin, E. Arda, Numerical simulation of transient heat transfer in friction-stir welding, International Journal of Heat and Technology, 2018, **36**, 26-30.
3. T. Sugihara, T. Enomoto, Development of a cutting tool with a nano micro textured surface -Improvement of anti-adhesiveeffect by considering the texture patterns. Precision Engineering, 2009, **33**, 425–429.
4. T. Sugihara, Y. Nishimoto, T. Enomoto, Development of a novel cubic boron nitride cutting tool with a textured flank face for high-speed machining of Inconel 718. Precision Engineering, 2016, **48**, 75-82
5. J. Kümmel, D. Braun, J. Gibmeier, J. Schneider, C. Greiner, V. Schulze, A. Wanner, Study on micro texturing of uncoated cemented carbide cutting tools for wear improvement and built-up edge stabilization. Journal of Materials Processing Technology, 2015, **215**, 62–70.
6. Y.F. Yang, Y.S. Su, L. Li, N. He, W. Zhao, Performance of cemented carbide tools with microgrooves in Ti-6Al-4V titanium alloy cutting. International Journal of Advanced Manufacturing Technology, 2014, **76**(9-12), 1731-1738.
7. Y.Q. Xing, J.X. Deng, J. Zhao, G.D. Zhang, K.D. Zhang, Cutting performance and wear mechanism of nanoscale and microscale textured Al2O3/TiC ceramic tools in dry cutting of hardened steel. International Journal of Refractory Metals & Hard Materials, 2014, **43**, 46–58.

8. Y.Y. Liu, J.X. Den, F.F. Wu, R. Duan, X. Zhang, Y.H. Hou, Wear resistance of carbide tools with textured flank-face in dry cutting of green alumina ceramics. Aeronautical Manufacturing Technology, 2017, **372-373**, 91-103.

9. T. Obikawa, A. Kamio, H. Takaoka, A. Osada, Micro-texture at the coated tool face for high performance cutting. International Journal of Machine Tools & Manufacture, 2011, **51**, 966–972.

10. D.M. Kim, V. Bajpai, B.H. Kim, H.W Park, Finite element modeling of hard turning process via a micro-textured tool. International Journal of Advanced Manufacturing Technology, 2015, **78**(9-12), 1393-1405.

11. N. Kawasegi, H. Sugimori, H. Morimoto, N. Morita, I. Hori, Development of cutting tools with microscale and nanoscale textures to improve frictional behavior. Precision Engineering, 2009, **33**, 248-254.

12. J.F. Ma, N.H. Duong, S. Lei, 3D numerical investigation of the performance of microgroove textured cutting tool in dry machining of Ti-6Al-4V. International Journal of Advanced Manufacturing Technology. 2015, **79**(5-8), 1313-1323.

13. J.F. Ma, N.H. Duong, S. Lei, Numerical investigation of the performance of microbump textured cutting tool in dry machining of AISI 1045 steel. Journal of Manufacturing Processes, 2014, **19**, 194-204.

14. P. Koshy, J. Tovey, Performance of electrical discharge textured cutting tools. CIRP Annals - Manufacturing Technology, 2011, **60**, 153-156.

15. N. Kawasegi, K. Ozaki, N. Morita, K. Nishimura, M. Yamaguchi. Development and machining performance of a textured diamond cutting tool fabricated with a focused ion beam and heat treatment. Precision Engineering, 2017, **47**, 311–320.

16. A. Fatima, P.T. Mativenga, A comparative study on cutting performance of rake-flank face structured cutting tool in orthogonal cutting of AISI/SAE 414. International Journal of Advanced Manufacturing Technology, 2015.

17. W.L. Zhu, Y.Q. Xing, K.F. Ehmann, B.F. Ju, Ultrasonic elliptical vibration texturing of the rake face of carbide cutting tools for adhesion reduction. International Journal of Advanced Manufacturing Technology, 2015.

18. J. Xie, M.J. Luo, J.L. He, X.R. Liu, T.W. Tan, Micro-grinding of Micro-groove Array on Tool Rake Surface for Dry Cutting of Titanium Alloy. International journal of precision engineering and manufacturing, 2012, **13**(10), 1845-1852.

19. Y. Li, J.X. Deng, Y.S. Chai, W.L. Fan, Surface textures on cemented carbide cutting tools by micro EDM assisted with high-frequency vibration. International Journal of Advanced Manufacturing Technology, 2016, **82**, 2157-2165.

20. R.A. Seraj, A. Abdollah-Zadeh, M. Hajian, F. Kargar, R. Soltanalizadeh, Microstructural Evolution and Wear Resistance of Friction Stir-Processed AISI 52100 Steel, Metallurgical & Materials Transactions A, 2016, **47**(7):3564-3572.

21. X.X. Lv, H.Y. Liu, Y.B. Wang, Microstructure and Dry Sliding Wear Behavior of Mg-Y-Zn Alloy Modified by Laser Surface Melting, Journal of Materials Engineering & Performance, 2011, **20**(6), 1015-1022.

22. J.J. Hu, H.B. Xu, Y.F. Chen, C. Han, Analysis of Friction and Wear Properties of 40Cr by High Current Pulsed Electron Beam, China Surface Engineering, 2012, **25**(4), 107-111.

23. A.R. Natasha, J.A. Ghani, C.H. Che Haron, J. Syarif, A.H. Musfirah, Temperature at the Tool-Chip Interface in Cryogenic and Dry Turning of AISI 4340 Using Carbide Tool, International Journal of Simulation Modelling, 2016, **15**(2), 201-212

24. N.R. Mathivanan, N.M. Babu, K.V. Kumar, Empirical study on twisting force using Taguchi doe technique during drilling of hybrid FRP laminate, Revue des Composites et des Matériaux Avancés, 2018, **28**(2), 277-288.

25. R.J. Wen, H. Tan, F.Y. Zhang, The Optimization of Microstructures and Properties in Heat Affect Zone of the Base in Laser Solid Formed TC4. YingyongJiguang/applied Laser Technology, 2012, **32**(2), 91-95.

26. A.P.I. Popoola, O.S. Fatoba, O.M. Popoola, The Influence of Heat Treatment and Process Parameters Optimization on Hardness and Corrosion Properties of Laser Alloyed X12CrNiMo Steel. Silicon, 2016, 1-11.

****

MANIFESTĂRI ȘTIINȚIFICE / SCIENTIFIC EVENTS

73rd RILEM Annual Week & International Conference on Innovative materials for Sustainable Civil Engineering (IMSCE)

25-30.08.2019, Nanjing International Youth Cultural Centre, China

Topics:
- Fresh concrete and chemical admixtures
- Hydration and microstructure characterization
- Sustainable cementitious materials
- Deformation and crack controlling
- Durability and service life prediction
- Ultra-high performance cementitious materials
- Sustainable building materials (wood, asphalt, ceramic…)

****